THE JOURNAL OF PHYSICAL CHEMISTRY C
A JOURNAL OF THE AMERICAN CHEMICAL SOCIETY

pubs.acs.org/JPCC
Article

Elucidating the Catalytic Valorization of Ethanol over Hydroxyapatite for Sustainable Butanol Production: A First-Principles Mechanistic Study

Albert F. B. Bittencourt, Gustavo P. Valença, and Juarez L. F. Da Silva*

Cite This: https://doi.org/10.1021/acs.jpcc.4c03937
Read Online

ABSTRACT: The widespread concern about the burning of fossil fuels and its effects on the environment has driven our research efforts toward sustainable energy solutions. As a result, there is a strong drive to improve the eco-friendly production of chemical compounds sourced from renewable resources. Here, we report a first-principle mechanistic study of the conversion of ethanol to butanol using a hydroxyapatite (HAP) catalyst. Basically, we combined density functional theory calculations, the unity bond index-quadratic exponential potential approximation to analyze the reaction mechanism, and microkinetic simulations to address the influence of the kinetic parameters on the chemical distribution of formed species on the HAP catalyst. From our calculations and analyses, the sequence of elementary reaction steps follows the Guerbet reaction pathway, which involves ethanol dehydrogenation, aldol condensation, and subsequent hydrogenation steps. The results indicate that the bifunctional nature of the HAP surface is key to facilitate the initial dehydrogenation of ethanol and subsequent C−C coupling *via* aldol condensation, determining reactions to the formation of C_4 species. Furthermore, microkinetic analysis shows that butanol is the main product, with minimal formation of other C_4 byproducts. However, higher initial ethanol coverages decrease the rate of conversion because of limited active sites. The conversion of the aldol intermediate is crucial for efficient butanol production. These findings provide valuable information for the future development of HAP-based catalysts for sustainable biofuel production.

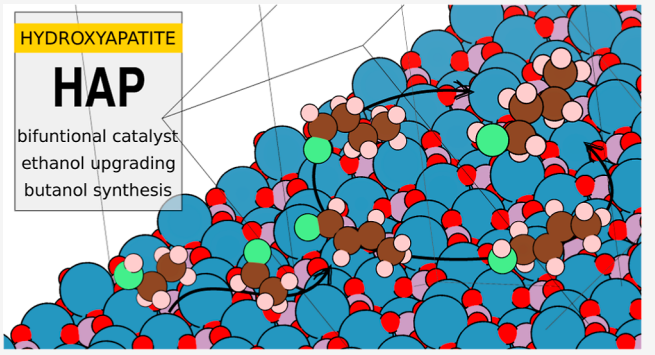

1. INTRODUCTION

Replacement of fossil fuels with renewable energy sources has become essential for the transition to a low carbon economy. To meet the challenge of addressing sustainability and energy security goals, significant efforts have been made in catalyst design and process development to convert biomass into fuels and high-value chemicals.[1−3] Recently, biobutanol production has emerged as a viable solution to accelerate the incorporation of sustainable biofuels into the energy economy.[4,5] Biobutanol has physicochemical properties similar to those of gasoline, making it an attractive option for internal combustion engines compared to other traditional fuels.[6,7] In addition, it can be obtained from a variety of biofeedstocks,[8,9] thus promoting the use of renewable resources and decreasing the dependence on petroleum-based fuels.

Given the challenges encountered in the fermentation-based production of butanol,[10] sustainable routes based on the Guerbet chemistry have also been explored as an alternative process to convert ethanol into butanol.[11,12] A key advancement in this field was the identification of hydroxyapatite [HAP, $Ca_{10}(PO_4)_6(OH)_2$] as an effective catalyst for the ethanol-to-butanol process.[13,14] In addition to being sustainable, this material exhibits unique bifunctional properties that can be adjusted by changing the surface distribution of acidic and basic sites, allowing the tuning of conversion and selectivity.[15,16] As a result, increasing importance has been placed in describing the surface chemistry of HAP[17] and its impact on the elementary reactions that compose the ethanol upgrading mechanism to butanol.[18]

Consistently, it has been demonstrated that the Guerbet mechanism consists of four main steps: (i) ethanol dehydrogenation to acetaldehyde, (ii) aldol condensation from two acetaldehyde molecules, (iii) crotonaldehyde formation, and (iv) consecutive hydrogenation reactions to form butanol.[19] However, a clear understanding of the HAP active sites involved in this process is still under debate. For instance, both CaO/PO_4^{3-}[20] and POH/OH^-[21,22] acidic−basic

Received: June 13, 2024
Revised: August 8, 2024
Accepted: August 14, 2024

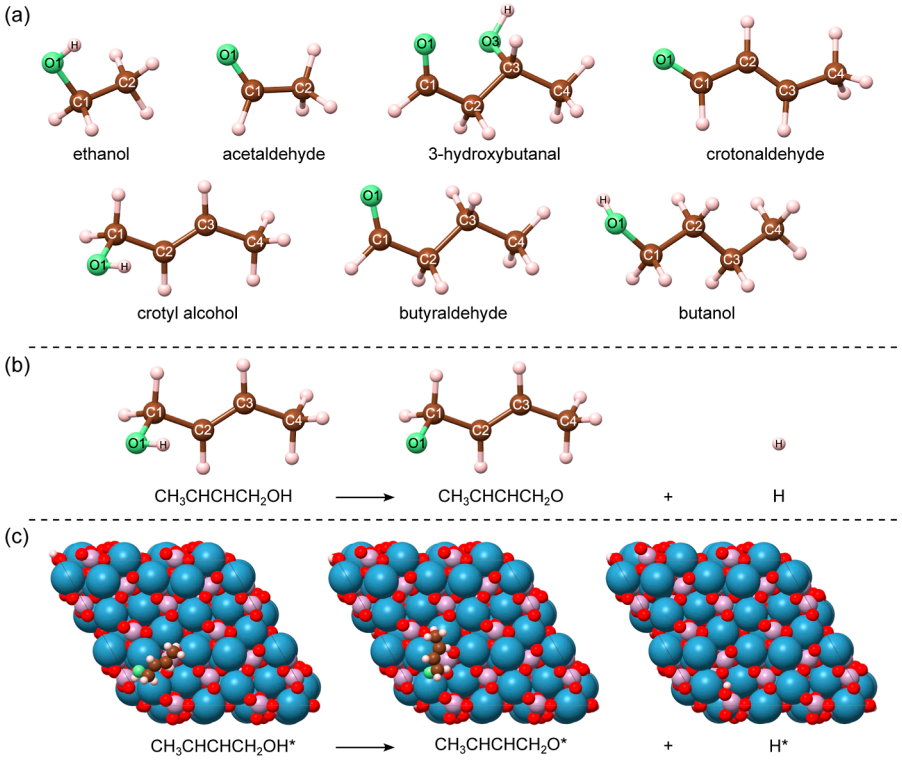

Figure 1. (a) Ball-and-stick representation of isolated gas-phase molecules used for the modeling of adsorption structure configurations. (b) A schematic representation of a dissociation reaction considered in the mechanism. (c) Space-filling representation of adsorption configurations on a 2 × 2 surface unit cell used to evaluate elementary reactions. Color reference: blue, red, and light pink spheres represent Ca, O, and P atoms in the substrate; brown, light green, and white spheres represent C, O, and H atoms in the molecules.

pairs have been suggested to be the active sites most responsible for the aldol condensation step. Contrarily, recent *operando* diffuse reflectance infrared Fourier transform spectroscopy measurements showed that the Ca^{2+}/OH^{-}[23] acidic−basic pairs govern the carbon−carbon coupling reaction. For the dehydrogenation of ethanol to acetaldehyde, different acidic−basic pairs have been identified as active sites, such as Ca−O[20] and Ca^{2+}/OH^{-}[22] species.

Because reaction rates depend on the surface chemistry of the catalyst, understanding the nature of HAP acidic−basic sites and their involvement in each elementary reaction plays an important role in the design of improved HAP-based catalysts. In this context, theoretical calculations can be useful in rationalizing the structure−reactivity relationship that exists in the catalytic valorization of ethanol on the HAP surface. In this study, we report a mechanistic study based on density functional theory (DFT) calculations to elucidate the reaction network of butanol synthesis on the HAP(0001) surface from an atomistic point of view. On the basis of the energetics of reaction intermediates, activation barriers were used to estimate kinetic properties and analyze how process parameters could influence the overall reaction mechanism and the distribution of formed species.

2. THEORETICAL APPROACH AND COMPUTATIONAL DETAILS

2.1. Total Energy Calculations. Our total energy calculations were performed within the spin-polarized DFT[24,25] framework, using the semilocal formulation proposed by Perdew−Burke−Ernzerhof for the exchange−correlation energy functional.[26] To solve the Kohn−Sham equations,[25] we used plane-wave basis sets and the frozen-core projector augmented wave (PAW) method[27,28] to describe the interaction among the core and valence electrons, as implemented in the Vienna *ab initio* simulation package (VASP), version 5.4.1.[29,30] To improve the description of nonlocal weak van der Waals interactions, we used the Grimme D3 semiempirical correction,[31] which is widely used to improve the description of adsorption processes.[32−34]

To ensure the precision required to describe the adsorption of molecular species on solid surfaces, all calculations used a plane-wave cutoff energy of 489 eV, which exceeds the maximum recommended plane-wave cutoff energy by 12.5% considering all selected PAW projectors. To obtain equilibrium structures, which play a crucial role in the quality of the results, we used convergence thresholds of 10^{-5} eV for the total energy and 0.025 eV $Å^{-1}$ for the residual force components in each atom. The integration of the Brillouin zone was carried out using only the Γ-point due to the size of the surface unit cell, which is defined below.

2.2. Atomic Structure Configurations. As well described in the literature, materials based on the HAP substrate exhibit a complex distribution of surface species due to their composition and structural arrangement.[18,35,36] Our modeling of HAP was based on our previous experience using this material as a catalyst. For example, by integrating experimental and theoretical calculations, we previously investigated the impact of synthesis conditions on the HAP surface and its catalytic properties.[37] Our findings demonstrated that the choice of the stoichiometric HAP(0001) surface is suitable for capturing its bifunctional properties and modeling ethanol catalysis, aligning with both experimental observations and theoretical predictions.

https://doi.org/10.1021/acs.jpcc.4c03937
J. Phys. Chem. C XXXX, XXX, XXX−XXX

To this end, in this study the stoichiometric termination HAP(0001) was selected to model the HAP surface in this study. We constructed a 1 × 1 surface unit cell based on the hexagonal bulk structure of HAP,[38] with dimensions of $a_0 = b_0$ = 9.497 Å, four formula units $Ca_5(PO_4)_3(OH)$ comprising a total of 88 atoms, a thickness of 12.88 Å, and a vacuum region of 15 Å. Because HAP catalysts exhibit bifunctional properties, the screening process was performed taking into account the existence of Ca^{2+} ions and PO_4^{3-} groups interspersed on the HAP(0001) surface. These chemical species act as positively and negatively charged chemical environments, for example, Lewis acidic and Lewis basic sites, respectively.[17]

To search for the lowest-energy adsorption configurations, we first generated a total of 30 distinct structures for each adsorption system (molecule) considered in the reaction mechanism. At this stage, the 1 × 1 surface unit cell was used to allow exploration at a reasonable computational cost. Then, after identifying the lowest energy configurations, each adsorption system was reoptimized using a 2 × 2 surface unit cell, as shown in Figure 1c. This slab model has a total of 352 atoms and increased lattice parameters of $a_0 = b_0$ = 18.995 Å, which minimizes the interaction between periodic images, allowing the estimation of zero-coverage adsorption energies. All adsorption structures were constructed by placing adsorbates symmetrically on both sides of the slab in equivalent positions, thus eliminating the need for dipole corrections. Furthermore, the initial geometries of the isolated gas-phase molecules, depicted in Figure 1a, were obtained from the PubChem database[39] and subsequently optimized them within a 20 Å cubic box. Full optimization was carried out for all investigated systems.

2.3. Estimation of Activation Energies. Recent literature has highlighted the usefulness of the unity bond index-quadratic exponential potential (UBI-QEP) approximation[40−42] in estimating activation energies for a proposed reaction mechanism, thus offering valuable insights on reactivity trends across different systems.[43−46] Within this approach, the activation energy of an elementary reaction is primarily estimated by adsorption and gas-phase bond dissociation energies, as described by

$$E_a = \frac{1}{2}\left(\Delta H_r + \frac{Q_A Q_B}{Q_A + Q_B}\right) \quad (1)$$

where ΔH_r, the surface reaction enthalpy, is computed as

$$\Delta H_r = Q_{AB} + D_{AB} - Q_A - Q_B \quad (2)$$

The energy of dissociation of the gas-phase bond, D_{AB}, corresponds to the energy required to break the gas-phase molecule AB into two separate fragments A and B, as illustrated in Figure 1b. Meanwhile, Q_{AB}, Q_A, and Q_B correspond to the adsorption energies used to estimate the strength of the interactions between these compounds and the catalyst surface. For example, in the dissociation reaction depicted in Figure 1c, the adsorbate $CH_3CHCHCH_2OH$* (crotyl alcohol) breaks into fragments $CH_3CHCHCH_2O$* + H* on the HAP(0001) surface. Here, Q_{AB} corresponds to the adsorption energy of the $CH_3CHCHCH_2OH$ molecule, while Q_A and Q_B correspond to the adsorption energies of $CH_3CHCHCH_2O$ and H fragments, respectively.

From this perspective, the adsorption energy Q_{AB} is calculated as

$$Q_{AB} = \frac{1}{2}(E_{tot}^{AB/Sub} - E_{tot}^{Sub} - 2E_{tot}^{AB}) \quad (3)$$

where $E_{tot}^{AB/Sub}$ is the total energy of the AB adsorbate, E_{tot}^{Sub} is the total energy of the clean HAP(0001) slab model, and E_{tot}^{AB} is the total energy of the AB molecule in the gas-phase. For the adsorption energies Q_A and Q_B, the coadsorption effect was considered to maintain the energetic consistency of the reaction mechanism, *e.g.*, in the case of a dissociation reaction, the resulting fragments are adsorbed at neighboring sites, which influences their interaction strengths with the substrate. Therefore, these parameters are defined as

$$Q_A = \frac{1}{2}(E_{tot}^{A+B/Sub} - E_{tot}^{B/Sub} - 2E_{tot}^{A}) \quad (4)$$

$$Q_B = \frac{1}{2}(E_{tot}^{A+B/Sub} - E_{tot}^{A/Sub} - 2E_{tot}^{B}) \quad (5)$$

where $E_{tot}^{A+B/Sub}$ represents the total energy of the coadsorbed system, $E_{tot}^{A/Sub}$ and $E_{tot}^{B/Sub}$ are the total energies of the fragments A and B separately adsorbed at the zero coverage limit, and E_{tot}^{A} and E_{tot}^{B} denote the total energy of the A and B gas-phase fragments, respectively. The terms $\frac{1}{2}$ and 2 in eqs 3−5 arise from placing adsorbates on both sides of the slab, according to the procedures defined above.

Thermodynamic properties obtained directly from DFT calculations are typically determined at a temperature of 0 K. To incorporate temperature effects into our mechanistic investigation, we considered the vibrational frequencies of the adsorbate species to estimate these properties.[47] Vibrational frequency calculations were conducted using the numerical finite difference method, with a convergence threshold set at 10^{-6} eV for total energy. It should be noted that small vibration frequencies significantly contribute to entropy; therefore, any frequency modes below 50 cm^{-1} were adjusted to 50 cm^{-1}.[48,49] The temperature of the reaction system was set to the actual reaction temperature of 573.15 K. All thermochemical properties were calculated using the thermochemistry module available in the atomic simulation environment software package.[50] Further details regarding the expression for activation energy and thermochemical corrections can be found in the Supporting Information, specifically in Sections S3 and S4.

2.4. Mechanistic Proposal. The proposed reaction mechanism is based on well-established research, which indicates that ethanol valorization on HAP-based catalysts primarily follows a Guerbet coupling pathway.[15,20,23,51−53] This pathway is typically divided into four key reaction steps:

- Acetaldehyde formation *via* ethanol dehydrogenation;
- C−C coupling *via* aldol condensation;
- Crotonaldehyde formation *via* dehydration;
- Subsequent hydrogenation reactions leading to butanol formation.

In this study, a total of 25 elementary reactions were proposed to encompass the upgrade of ethanol to butanol on the HAP(0001) surface. To provide a comprehensive description, all elementary reactions are detailed in Table 1. In our mechanistic investigation, the elementary reactions that describe crotonaldehyde formation are designated as R_1 to R_7, with a graphical representation provided in Figure 2. In subsequent hydrogenation reactions, two potential reaction pathways were considered: (i) butanol formation *via* crotyl alcohol (reactions R_8 to R_{16}), and (ii) butanol formation *via*

https://doi.org/10.1021/acs.jpcc.4c03937
J. Phys. Chem. C XXXX, XXX, XXX−XXX

Table 1. Selected Series of Elementary Reactions on the HAP(0001) Surface for Investigating Butanol Synthesis through the Conversion of Ethanol

reaction pathway	label	elementary reaction
acetaldehyde formation	R_1	$CH_3CH_2OH^* + * \rightleftarrows CH_3CH_2O^* + H^*$
	R_2	$CH_3CH_2O^* + * \rightleftarrows CH_3CHO^* + H^*$
enolate formation	R_3	$CH_3CHO^* + * \rightleftarrows CH_2CHO^* + H^*$
aldol condensation	R_4	$CH_3CHOCH_2CHO^* + * \rightleftarrows CH_2CHO^* + CH_3CHO^*$
	R_5	$CH_3CHOHCH_2CHO^* + * \rightleftarrows CH_3CHOCH_2CHO^* + H^*$
crotonaldehyde formation	R_6	$CH_3CHOHCH_2CHO^* + * \rightleftarrows CH_3CHCH_2CHO^* + OH^*$
	R_7	$CH_3CHCH_2CHO^* + * \rightleftarrows CH_3CHCHCHO^* + H^*$
crotyl alcohol formation	R_8	$CH_3CHCHCHO^* + CH_3CH_2OH^* \rightarrow CH_3CHCHCH_2OH^* + CH_3CHO^*$
	R_9	$CH_3CHCHCH_2O^* + * \rightleftarrows CH_3CHCHCHO^* + H^*$
	R_{10}	$CH_3CHCHCH_2OH^* + * \rightleftarrows CH_3CHCHCH_2O^* + H^*$
	R_{11}	$CH_3CHCHCHOH^* + * \rightleftarrows CH_3CHCHCHO^* + H^*$
	R_{12}	$CH_3CHCHCH_2OH^* + * \rightleftarrows CH_3CHCHCHOH^* + H^*$
butanol formation *via* crotyl alcohol	R_{13}	$CH_3CH_2CHCH_2OH^* + * \rightleftarrows CH_3CHCHCH_2OH^* + H^*$
	R_{14}	$CH_3CH_2CH_2CH_2OH^* + * \rightleftarrows CH_3CH_2CHCH_2OH^* + H^*$
	R_{15}	$CH_3CHCH_2CH_2OH^* + * \rightleftarrows CH_3CHCHCH_2OH^* + H^*$
	R_{16}	$CH_3CH_2CH_2CH_2OH^* + * \rightleftarrows CH_3CHCH_2CH_2OH^* + H^*$
butyraldehyde formation	R_{17}	$CH_3CH_2CHCHO^* + * \rightleftarrows CH_3CHCHCHO^* + H^*$
	R_{18}	$CH_3CH_2CH_2CHO^* + * \rightleftarrows CH_3CH_2CHCHO^* + H^*$
	R_{19}	$CH_3CHCH_2CHO^* + * \rightleftarrows CH_3CHCHCHO^* + H^*$
	R_{20}	$CH_3CH_2CH_2CHO^* + * \rightleftarrows CH_3CHCH_2CHO^* + H^*$
butanol formation *via* butyraldehyde	R_{21}	$CH_3CH_2CH_2CH_2O^* + * \rightleftarrows CH_3CH_2CH_2CHO^* + H^*$
	R_{22}	$CH_3CH_2CH_2CH_2OH^* + * \rightleftarrows CH_3CH_2CH_2CH_2O^* + H^*$
	R_{23}	$CH_3CH_2CH_2CHOH^* + * \rightleftarrows CH_3CH_2CH_2CHO^* + H^*$
	R_{24}	$CH_3CH_2CH_2CH_2OH^* + * \rightleftarrows CH_3CH_2CH_2CHOH^* + H^*$
	R_{25}	$CH_3CH_2CH_2CHO^* + CH_3CH_2OH^* \rightarrow CH_3CH_2CH_2CH_2OH^* + CH_3CHO^*$

butyraldehyde (reactions R_{17} to R_{25}). Visual representations of these reaction steps are depicted in Figure 4.

2.5. Microkinetic Model Simulation. Microkinetic simulation is a useful tool that can help in understanding heterogeneous catalytic processes,[54] allowing the determination of reaction rates for individual elementary reactions and the coverage of intermediate species on the catalyst surface under actual operating conditions.[55] For the simulation of the microkinetic model used in this study, we considered that all adsorption sites are identical and can adsorb only one adsorbate species at a time. Then, once the activation energies for the proposed forward and reverse elementary reactions were obtained using the UBI-QEP method described above, the rate constants were assumed to have the Arrhenius form

$$k = A \exp\left(\frac{-E_a}{RT}\right) \tag{6}$$

with the pre-exponential factor determined as[56]

$$A = \frac{k_b T}{h} \exp\left(\frac{\Delta S^{\ddagger}}{R}\right) \tag{7}$$

where k_b is the Boltzmann's constant, h is Planck's constant, $\Delta S^{\ddagger}$ is the entropy change from the reactant to the transition state complex, E_a is the activation energy, R is the universal gas constant, and T is the reaction temperature.

For each elementary reaction labeled as R_i, the reaction rate is expressed as the sum of the forward and reverse reaction rates defined as $r_{i,f}$ and $r_{i,r}$, respectively. For example, in the case of reaction R_1, the forward and reverse reaction rates are written as

$$r_{1,f} = k_{1,f}\theta_{CH_3CH_2OH^*}\theta_* \tag{8}$$

$$r_{1,r} = k_{1,r}\theta_{CH_3CH_2O^*}\theta_{H^*} \tag{9}$$

where the quantities $k_{i,f}$ and $k_{i,r}$ correspond to the rate constants of forward and reverse reactions, while θ_j refers to the surface coverage of the species j involved in the elementary reaction R_1. For the overall reaction mechanism, a total of 22 species are defined, including vacancy sites.

As a consequence of the reaction rate, the surface coverage of each species j is affected over time. Therefore, we used the reaction rate expressions to determine surface coverage of each component in the form of a ordinary differential equation

$$\frac{d}{dt}\theta_{j^*} = \sum_i \nu_{j,i} r_i \tag{10}$$

where $\nu_{j,i}$ is the dimensionless stoichiometric coefficient of species j in elementary reaction i. To obtain the steady-state values of surface coverages, the entire set of ordinary differential equations was numerically integrated using the integrator subpackage available in the SciPy computing library.[57] Further details regarding the expression for forward and reverse reaction rates, as well as the entire set of ordinary differential equation can be found in the Supporting Information, Section S5.

3. RESULTS AND DISCUSSION

In this study, a comprehensive sequence of elementary reactions was proposed to evaluate butanol production through the upgrading of ethanol on the HAP(0001) surface. Here, our focus lies on the primary findings concerning the reaction pathways. We delve into the physical−chemical properties of the reaction intermediates and explore the activation energies involved in the catalytic process. On the basis of the estimated kinetic parameters, we also provided valuable insights into the reaction mechanism from a microkinetic perspective. To help in the discussion of our results, Table 2 presents the activation energies for each elementary reaction. Additionally, Figure 3 illustrates a free energy diagram for the pathway in which ethanol is converted to crotonaldehyde, as depicted in Figure 2. For supporting analysis, the results of the gas-phase molecules and the substrate slab model are provided in the Supporting Information, Section S2. Furthermore, selected properties of the adsorbed species are organized in Section S6.

https://doi.org/10.1021/acs.jpcc.4c03937
J. Phys. Chem. C XXXX, XXX, XXX−XXX

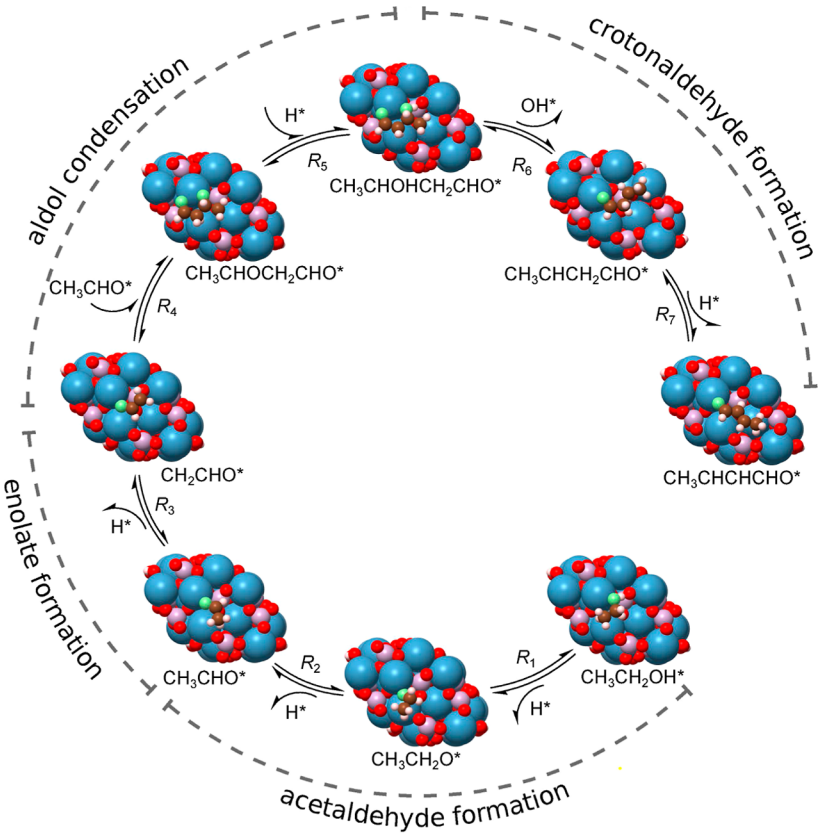

Figure 2. Proposed sequence of elementary reactions for obtaining crotonaldehyde on the HAP(0001) surface. The proposed reaction pathway encompasses the acetaldehyde formation (R_1 and R_2), the enolate formation (R_3), the aldol condensation (R_4 and R_5), and the crotonaldehyde formation (R_6 and R_7). All reactions are detailed in Table 1.

3.1. Acetaldehyde Formation. In the Guerbet mechanism, butanol synthesis is based on the formation of acetaldehyde molecules through the dehydrogenation of ethanol. Our theoretical findings indicate a nondissociative adsorption of ethanol on the HAP(0001) surface. The most energetically stable adsorption configuration of ethanol ($CH_3CH_2OH^*$) exhibits an adsorption free energy of −1.19 eV at 573.15 K. In this configuration, the adsorption is primarily influenced by the hydroxyl group. An acidic site (Ca^{2+} ion) attracts the oxygen atom at a distance of 2.35 Å, while a neighboring basic site (PO_4^{3-} group) attracts the hydrogen atom at a distance of 1.68 Å. As a result, hydroxyl O−H bond is elongated from 0.97 to 1.01 Å.

In addition, the redistribution of charges resulting from the interaction between the adsorbate and the substrate induces a depletion of charges around the hydrogen atom (see the analysis of electron density differences provided in the Supporting Information, Section S6, Table S11), consistent with the weakening of O−H bond necessary for the dehydrogenation of ethanol (reaction R_1, Figure 2). This first reaction was found to be endergonic by +0.37 eV, with an activation energy of 1.45 eV, leading to the formation of an ethoxide intermediate ($CH_3CH_2O^*$) and a hydrogen radical. Compared to the configuration of adsorbed ethanol, the resulting ethoxide is less stable in the HAP(0001) surface, with an adsorption free energy of −0.76 eV. This observation aligns with the dissociation of ethoxide considered in the reaction mechanism, which results in the formation of the acetaldehyde molecule (reaction R_2, Figure 2) through an exergonic reaction of −0.60 eV with a significantly lower activation energy of 0.17 eV.

3.2. Enolate Formation. The coexistence of acidic and basic sites on the HAP(0001) surface has a direct influence on stabilizing the formed acetaldehyde (CH_3CHO^*). On the one end, the molecule is drawn toward an acidic site as a result of the attraction of its carbonyl group. On the other end, a basic site attracts the hydrogen atom bonded to the C2 carbon atom. This adsorption configuration exhibits a noticeable charge rearrangement. There is an evident accumulation of charge between the carbonyl group and the Ca^{2+} ion, and a depletion of charge around the hydrogen atom bound to the C2 carbon atom in the acetaldehyde. This observation is also followed by an elongation of C2−H bond from 1.102 to 1.115 Å. This weakening of the bond is necessary for the formation of the enolate intermediate (CH_3CHO^*), which needs to surpass a reaction barrier of 1.26 eV (reaction R_3, Figure 2).

3.3. Aldol Condensation. As discussed previously, aldol condensation is generally accepted as the primary reaction pathway for C−C coupling within the Guerbet mechanism. This reaction involves the attack of the C2 in the enolate intermediate on the C1 of a neighboring acetaldehyde molecule (reaction R_4, Figure 2). Among the various adsorption configurations investigated for the enolate−acetaldehyde coadsorbed pair, the most energetically stable system exhibited each molecule adsorbed at neighboring sites with the carbonyl group oriented toward the Ca^{2+} ion. Their oxygen atoms interacted with the substrate at distances of 2.33 Å for the enolate and 2.39 Å for the acetaldehyde. Analysis of the electron density difference reveals a slight accumulation of

https://doi.org/10.1021/acs.jpcc.4c03937
J. Phys. Chem. C XXXX, XXX, XXX−XXX

Table 2. Activation Energies of the Elementary Reactions in the Butanol Synthesis *via* Ethanol Upgrading[a]

label	Q_A	Q_B	$\Delta H_{r,f}$	$E_{a,f}$	$E_{a,b}$
R_1	−5.98	−4.37	0.37	1.45	1.07
R_2	−3.01	−1.47	−0.64	0.17	0.81
R_3	−5.27	−3.92	0.27	1.26	0.99
R_4	−1.81	−1.99	−0.54	0.20	0.74
R_5	−6.79	−3.92	0.87	1.68	0.81
R_6	−5.69	−4.66	0.49	1.53	1.03
R_7	−4.09	−1.69	−0.56	0.32	0.88
R_8	−3.28	−2.00	0.27	0.76	0.48
R_9	−4.09	−1.69	−1.09	0.05	1.14
R_{10}	−6.85	−4.42	−0.08	1.30	1.38
R_{11}	−4.09	−1.69	0.13	0.66	0.54
R_{12}	−4.69	−2.08	1.05	1.24	0.20
R_{13}	−3.43	−0.63	1.28	0.91	0.00
R_{14}	−5.35	−2.42	1.82	1.74	0.00
R_{15}	−3.43	−0.63	1.37	0.95	0.00
R_{16}	−5.09	−2.10	2.05	1.77	0.00
R_{17}	−4.09	−1.69	−0.09	0.56	0.64
R_{18}	−6.05	−3.75	0.18	1.25	1.07
R_{19}	−4.09	−1.69	−0.69	0.26	0.94
R_{20}	−4.74	−2.64	1.90	1.80	0.00
R_{21}	−3.76	−1.24	−0.34	0.30	0.64
R_{22}	−6.96	−4.28	0.36	1.51	1.14
R_{23}	−3.76	−1.24	−0.19	0.37	0.56
R_{24}	−4.86	−2.39	2.10	1.85	0.00
R_{25}	−3.58	−1.95	0.02	0.64	0.62

[a] Q_A, Q_B, and $\Delta H_{r,f}$ represent the adsorption energies and the surface reaction enthalpy necessary to estimate the activation energies using the UBI-QEP method. All values are presented in eV.

electron density around C2 in enolate, accompanied by a more pronounced depletion of charge around the C1 in acetaldehyde. From an energetic standpoint, despite the lower stability observed for the enolate intermediate, its coadsorption free energy is comparable to that of acetaldehyde, with magnitudes of −0.42 and −0.58 eV for the enolate and acetaldehyde, respectively. The calculated activation energy for this elementary reaction was found to be 0.74 eV.

Following the C−C coupling, the electronic charge accumulates near the deprotonated oxygen in the adsorbate. This accumulation of electron density facilitates surface-mediated hydrogenation of the resulting C_4 product ($CH_3CHOCH_2CHO^*$) to form the aldol intermediate ($CH_3CHOHCH_2CHO^*$) (reaction R_5, Figure 2). This elementary reaction is exergonic by −0.86 eV and needs to overcome an activation barrier of 0.81 eV. The aldol compound formed exhibits higher stability on the HAP(0001) surface, as indicated by an adsorption free energy of −2.02 eV. This observation is consistent with the adsorption configuration obtained for the aldol compound, where both oxygen atoms interact with the positively charged Ca^{2+} ion. The carbonyl and hydroxyl groups within the molecule interact at distances of 2.39 and 2.34 Å, respectively. Furthermore, the hydroxyl group is further stabilized through interaction between its hydrogen atom and a surface-exposed oxygen atom within the PO_4^{3-} group.

3.4. Crotonaldehyde Formation. The aldol molecule then undergoes two consecutive elementary reactions to yield crotonaldehyde ($CH_3CHCHCHO^*$). In the first reaction, there is a breaking of the C3−OH bond (reaction R_6, Figure 2), as interactions between the OH group and the catalyst surface weaken the C3−OH bond. As mentioned, the oxygen atom interacts mainly with Ca^{2+} ion at a distance of 2.34 Å, while a nearby phosphate group attracts the hydrogen atom at a distance of 1.66 Å. In addition, analysis of the difference in electron density indicates that a region of charge depletion is observed between the OH group and the C3 atom. Despite the weakening of C3−OH bond, this reaction still needs to overcome a relatively higher reaction barrier of 1.53 eV, resulting in an endergonic final state by +0.50 eV. This elementary reaction produces an unstable intermediate ($CH_3CHCH_2CHO^*$) that is readily converted to crotonaldehyde through the subsequent abstraction of a H from C2 atom (reaction R_7, Figure 2). This reaction is thermodynamically favored, with an exergonic energy of −0.63 eV and a lower activation energy of 0.32 eV. Following the abstraction of H from C2, the unsaturated carbon chain is formed. This can be seen in the decrease in intramolecular C2═C3 bond length from 1.53 to 1.36 Å.

3.5. Crotyl Alcohol Formation. In our proposed reaction mechanism, two distinct hydrogenation pathways were considered for the formation of crotyl alcohol ($CH_3CHCHCH_2OH^*$). In the first pathway, the carbonyl group within the crotonaldehyde is directly hydrogenated through the H-transfer from a neighboring adsorbed ethanol molecule. Alternatively, in another reaction route, the carbonyl

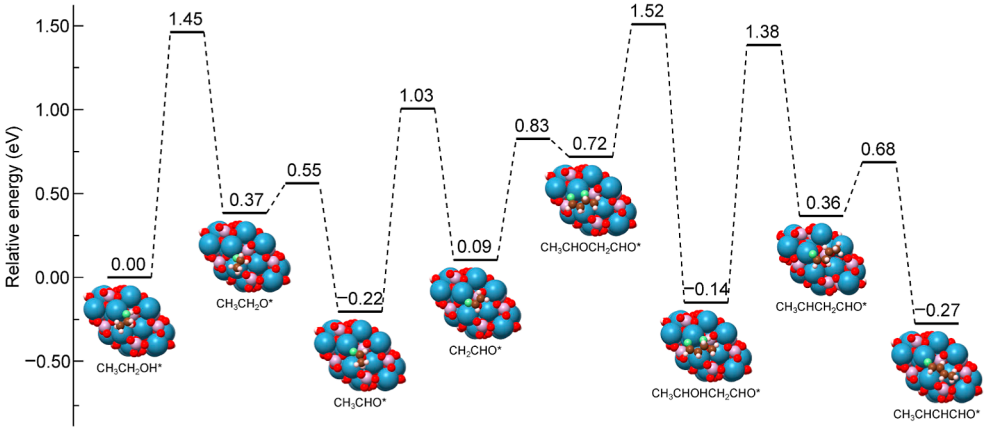

Figure 3. Free energy diagram for the proposed catalytic formation of crotonaldehyde from ethanol at 573.15 K.

https://doi.org/10.1021/acs.jpcc.4c03937
J. Phys. Chem. C XXXX, XXX, XXX−XXX

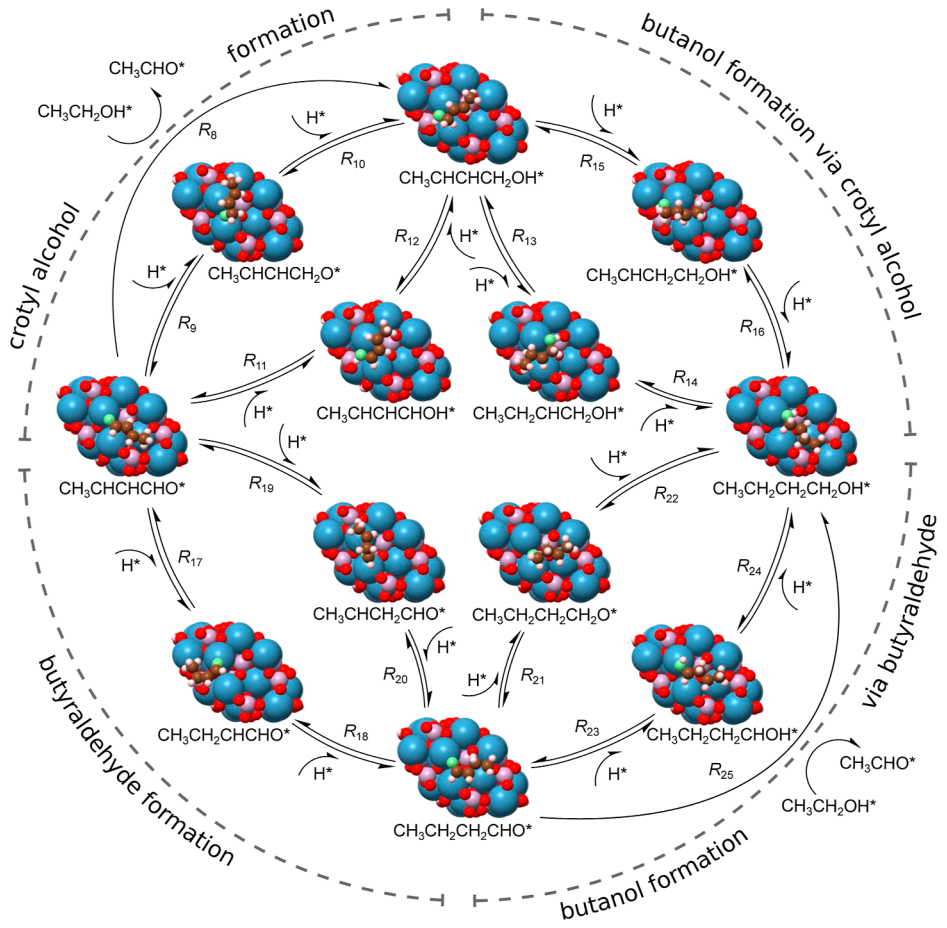

Figure 4. Proposed sequence of elementary reactions for the hydrogenation of crotonaldehyde to form butanol on the HAP(0001) surface. The proposed reaction pathway encompasses the crotyl alcohol formation (R_8 to R_{12}), the butanol formation *via* crotyl alcohol (R_{13} to R_{16}), the butyraldehyde formation (R_{17} to R_{20}), and the butanol formation *via* butyraldehyde (R_{21} to R_{25}). All reactions are detailed in Table 1.

group can undergo two consecutive surface-mediated hydrogenation reactions.

In the elementary reaction that represents hydrogenation *via* direct H-transfer from ethanol (reaction R_8, Figure 4), the most energetically stable system exhibits both crotonaldehyde and ethanol molecules adsorbed at neighboring sites, with the carbonyl and hydroxyl groups oriented toward Ca^{2+} ion at similar distances of 2.31 and 2.36 Å, respectively. Then, the ethanol molecule is dehydrogenated to acetaldehyde, and crotonaldehyde is converted to crotyl alcohol through the concerted breaking of O−H and C1−H bonds in ethanol and the migration of hydrogen to both carbon and oxygen atoms of the C1═O group in crotonaldehyde. Our findings indicate an endergonic elementary reaction (+0.26 eV) with moderate activation energy of +0.76 eV.

Two scenarios were explored for surface-mediated hydrogenation of the carbonyl group: (i) C1 hydrogenation of atoms followed by protonation of the oxygen atom, or (ii) the reverse sequence. In the first scenario, crotonaldehyde is converted to crotyl alcohol through the formation of a $CH_3CHCHCH_2O^*$ intermediate (reactions R_9 and R_{10}, Figure 4). Our findings indicate that both steps are endergonic reactions by +1.06 and +0.06 eV with activation energies of 1.14 and 1.38 eV, respectively. In the second scenario, crotonaldehyde is converted to crotyl alcohol through the formation of a $CH_3CHCHCH_2OH^*$ intermediate (reactions R_{11} and R_{12}, Figure 4). According to the energetics of the reactions, this pathway suggests that surface-mediated hydrogenation of crotonaldehyde that occurs through the oxygen atom in carbonyl is a more thermodynamically stable route, in which both steps are exergonic by −0.12 and −1.09 eV with lower activation energies of 0.54 and 0.20 eV, respectively.

3.6. Butanol Formation *via* Crotyl Alcohol. The surface-mediated hydrogenation approach was also considered for the formation of butanol ($CH_3CH_2CH_2CH_2OH^*$) from crotyl alcohol, considering two different pathways. The unsaturated C2═C3 bond can undergo hydrogenation, initiating either at C2 or C3 atoms in the crotyl alcohol (reactions R_{13}, R_{14}, R_{15}, and R_{16}, Figure 4). In this scenario, all elementary reactions exhibited an energy barrier of 0.00 eV. As noted by Shustorovich, the UBI-QEP method may produce physically meaningless negative activation barriers, particularly in scenarios where the surface reaction is highly exothermic or the gas-phase species is exceptionally unstable.[42] In our study, while the energy required to dissociate the investigated bonds was positive, all elementary reactions considered in this pathway were noticeably exergonic, with values ranging from −1.26 to −2.09 eV. Therefore, we were unable to identify the activation energies for these steps.

3.7. Butyraldehyde Formation. An alternative reaction pathway involves the formation of butyraldehyde, where the crotonaldehyde molecule undergoes hydrogenation at the unsaturated C2═C3 bond rather than the carbonyl group. Similarly, the unsaturated bond can be hydrogenated starting

https://doi.org/10.1021/acs.jpcc.4c03937
J. Phys. Chem. C XXXX, XXX, XXX−XXX

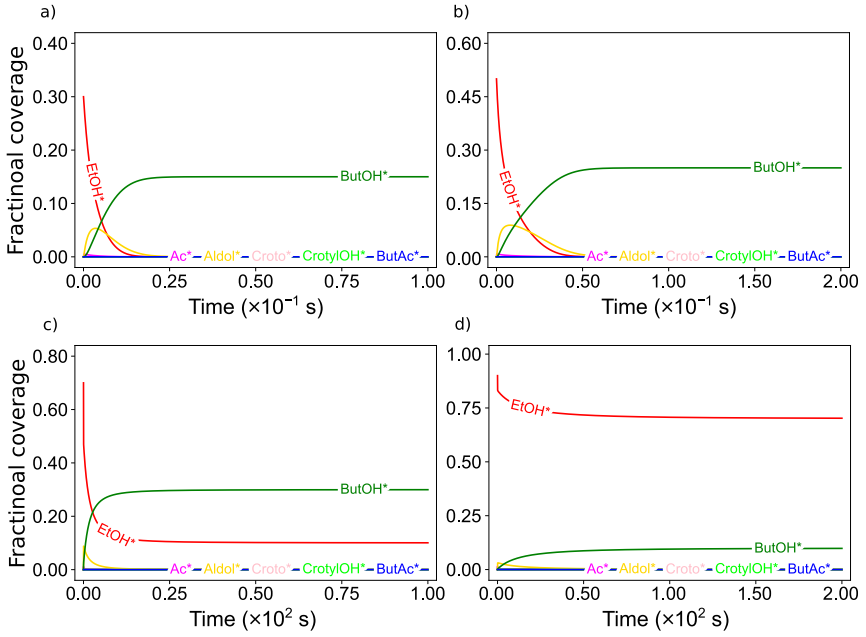

Figure 5. Microkinetic simulation results showing the influence of initial ethanol concentration on the surface distribution of formed species. The fractional coverages of ethanol considered are (a) 0.3, (b) 0.5, (c) 0.7, and (d) 0.9. The main reaction species displayed are ethanol (EtOH), acetaldehyde (Ac), 3-hydroxybutanal (Aldol), crotonaldehyde (Croto), crotyl alcohol (CrotylOH), butyraldehyde (ButAc), and butanol (ButOH).

at either the C2 or C3 carbon atoms. When comparing the energetics of both scenarios, surface-mediated hydrogenation starting at C3 atom (reactions R_{17} and R_{18}, Figure 4) involves the formation of a $CH_3CH_2CHCHO^*$ intermediate through a slightly exergonic reaction by +0.07 eV, with an activation energy of 0.64 eV, followed by a subsequent hydrogenation (exergonic by −0.20 eV) with a higher activation barrier of 1.07 eV. In contrast, surface-mediated hydrogenation starting at C2 atom (reactions R_{19} and R_{20}, Figure 4) forms a $CH_3CHCH_2CHO^*$ intermediate. This elementary reaction must surpass an activation barrier of 0.94 eV, while subsequent hydrogenation has an activation energy equal to 0.00 eV. Here, the activation energy value falls into the physically meaningless situation of having a negative activation barrier because of the strongly exothermic character, as mentioned above.

3.8. Butanol Formation *via* Butyraldehyde. Two distinct mechanisms for the hydrogenation of butyraldehyde to butanol were investigated. The first pathway involves surface-mediated hydrogenation of the carbonyl group, while the second considers an ethanol molecule as a hydrogen source *via* direct H-transfer.

For the surface-mediated hydrogenation mechanism, the first pathway involves hydrogenation at C1 atom of butyraldehyde, followed by the protonation of the oxygen atom (reactions R_{21} and R_{22}, Figure 4). This sequence begins with an endergonic step (+0.32 eV), followed by an exergonic step (−0.39 eV), with activation energy barriers of 0.64 and 1.14 eV, respectively. Alternatively, the process can begin with hydrogenation of the oxygen atom followed by C1 hydrogenation (reactions R_{23} and R_{24}, Figure 4). In this scenario, an endergonic step (+0.14 eV) is followed by a significantly more exergonic reaction (−2.07 eV). These elementary reactions have an activation energy of 0.56 and 0.00 eV, respectively. The UBI-QEP approach predicts a null activation energy for highly exothermic reactions, consistent with the observed case.

When considering direct H-transfer from ethanol, butyraldehyde is hydrogenated to form butanol, while ethanol is converted into acetaldehyde (reaction R_{25}, Figure 4). The concerted activation energy for this reaction is 0.62 eV. Interestingly, the adsorbed configuration of the butanol molecule is similar to that of ethanol. The substrate interacts with the OH group *via* an acidic−basic interaction, where the Ca^{2+} ion attracts the oxygen atom at a distance of 2.34 Å, and a neighboring phosphate group attracts the hydrogen atom at a distance of 1.68 Å. This simultaneous interaction weakens the bond O−H, as evidenced by its increased length from 0.97 to 1.01 Å, along with the observed charge depletion around the hydrogen atom.

3.9. Microkinetic Analysis. Microkinetic modeling is a powerful tool for determining important kinetic parameters and providing valuable insights that complement and extend experimental findings. To gain a deeper atomistic understanding of the ethanol coupling reaction and how kinetic parameters could influence the general distribution of formed species on the HAP(0001) surface, we conducted microkinetic simulations based on the well-established Guerbet mechanism for butanol synthesis. These simulations were performed at a reaction temperature of 573.15 K and atmospheric pressure to replicate the actual experimental conditions.[37]

Our focus was on examining how the initial concentration of ethanol adsorbed on the catalyst surface affects the final coverage of the formed species once a steady state is reached (a point in time where the concentrations of all species remain constant). Specifically, four different initial fractional coverages of ethanol were investigated, including 0.3, 0.5, 0.7, and 0.9. The simulation results showing the coverage profile over time are presented in Figure 5, while the specific rate constants for each elementary reaction are provided in the Supporting Information, Section S5, Table S6.

As expected, butanol emerged as the main product at steady state, consistent with experimental observations.[23,37,58] Wang *et al.* demonstrated using modulation excitation spectroscopy that introducing ethanol into the reaction system results in small amounts of intermediates such as acetaldehyde,

https://doi.org/10.1021/acs.jpcc.4c03937
J. Phys. Chem. C XXXX, XXX, XXX−XXX

crotonaldehyde, crotyl alcohol, and butyraldehyde.[23] Our findings indicate a slight increase in acetaldehyde concentration during the initial stages, followed by a gradual increase in the aldol intermediate concentration. This observation strongly aligns with the steady-state isotopic transient kinetic analysis performed by Hanspal *et al.*,[58] which revealed that the surface coverage of reaction intermediates leading to acetaldehyde is much lower than that leading to butanol.

For all investigated scenarios, our microkinetic model indicates that a maximum in butanol coverage corresponds to a minimum in the aldol intermediate, which is consistent with the observed experimental trends.[23] Aldol condensation is a key reaction step in the Guerbet mechanism, where longer carbon chains are formed by coupling through aldol condensation. Consequently, butanol formation continues as long as the aldol intermediate is available on the catalyst surface. As illustrate in Figure 5, the butanol coverage profile keeps increasing until the aldol intermediate is completely converted. Interestingly, the presence of other C_4 intermediate compounds, such as crotonaldehyde, crotyl alcohol, and butyraldehyde, was negligible, suggesting a strong preference for butanol formation compared to the other products.[23,37]

Furthermore, higher initial ethanol concentrations lead to a decrease in its conversion. For initial fractional coverages of 0.3 and 0.5, ethanol is completely converted into butanol. An initial fractional coverage of 0.7, a conversion of 86% is achieved, while only 22% of ethanol is converted for an initial fractional coverage of 0.9. This observation can be attributed to the limited availability of vacancy sites for participation in the reaction mechanism as more molecules are adsorbed on the catalyst surface.

To evaluate the robustness of our microkinetic simulation, we examined the influence of random errors introduced into the calculated adsorption energies. These deviations were specifically analyzed in the context of adsorption energies because of their critical role in estimating kinetic parameters and their potential to reflect deviations observed in theoretical *versus* experimental values. For the initial fractional coverage of 0.3 and 0.5, deviations of up to 10% had minimal impact on the surface distribution of adsorbed species. However, for initial fractional coverages of 0.7 and 0.9, deviations exceeding 5% in adsorption energies, it began to noticeably affect the conversion of ethanol and surface distribution. Overall, an increase in the random error values resulted in decreased ethanol conversion, followed by a primarily increased concentration of the ethoxide intermediate. The abundance of other intermediate compounds remained largely unchanged. The fractional coverage of each intermediate species is provided in Tables S7 to S10 in the Supporting Information.

4. CONCLUSIONS

In this work, we used DFT calculations to elucidate the catalytic upgrading of ethanol to butanol on the hydroxyapatite (0001) surface. A comprehensive description of the Guerbet mechanism on this catalyst is provided at the atomic level, providing valuable insights into the surface chemistry that governs this conversion process. By evaluating the energetics and activation energy barriers of the elementary steps, we performed microkinetic simulations to elucidate how the initial coverage of ethanol on the surface affects the distribution of the formed products.

The proposed reaction mechanism highlights the important role of the acidic−basic properties of hydroxyapatite in the facilitation of various elementary reactions. For example, the initial dehydrogenation of ethanol and the subsequent coupling of C−C through aldol condensation determine reactions to the formation of C_4 species. Our calculations indicate that the surface readily facilitates the conversion of these intermediates to butanol. Notably, butanol formation from crotonaldehyde can occur through two distinct hydrogenation pathways: *via* crotyl alcohol or butyraldehyde. Furthermore, direct H-transfer from ethanol and surface-mediated hydrogenation reactions may compete as mechanisms for the hydrogenation of intermediate species.

Microkinetic simulations revealed butanol as the main product obtained with minimal formation of other C_4 byproducts such as crotonaldehyde, crotyl alcohol, and butyraldehyde. By evaluation of the initial ethanol concentration, we observed that higher ethanol coverages on the catalyst surface limit the availability of active sites, which results in a decreased conversion of ethanol. Another significant observation is that the conversion of the aldol intermediate is a key to butanol formation. These insights are expected to be valuable in the development of novel hydroxyapatite-based catalysts aimed at enhancing sustainable butanol production from ethanol.

■ ASSOCIATED CONTENT

Data Availability Statement

Additional details supporting the findings of this study are available in the Supporting Information accompanying this document. This includes selected properties of adsorbed species, a comprehensive description of the microkinetic simulation and activation energy calculations, an overview of the applied thermochemical corrections, and the complete set of structures evaluated. For further details, please contact the corresponding author.

Supporting Information

The Supporting Information is available free of charge at https://pubs.acs.org/doi/10.1021/acs.jpcc.4c03937.

S1: Additional details on the PAW projectors. S2: Gas-phase molecules and the slab model. S3: Estimation of activation energies using the UBI-QEP. S4: Thermochemical analysis and vibrational frequencies. S5: Microkinetic model simulation. S6: Adsorption properties of selected species. S7: Complete set of adsorption structures. S8: POSCAR files (PDF)

■ AUTHOR INFORMATION

Corresponding Author

Juarez L. F. Da Silva − *São Carlos Institute of Chemistry, University of São Paulo, 13560-970 São Carlos, São Paulo, Brazil;* orcid.org/0000-0003-0645-8760; Email: juarez_dasilva@iqsc.usp.br

Authors

Albert F. B. Bittencourt − *São Carlos Institute of Chemistry, University of São Paulo, 13560-970 São Carlos, São Paulo, Brazil;* orcid.org/0000-0002-9418-0166

Gustavo P. Valença − *School of Chemical Engineering, University of Campinas, 13083-852 Campinas, São Paulo, Brazil*

Complete contact information is available at: https://pubs.acs.org/10.1021/acs.jpcc.4c03937

Funding

The Article Processing Charge for the publication of this research was funded by the Coordination for the Improvement of Higher Education Personnel - CAPES (ROR identifier: 00x0ma614).

Notes

The authors declare no competing financial interest.

■ ACKNOWLEDGMENTS

The authors appreciate the support from FAPESP (São Paulo Research Foundation) and Shell, grant numbers 2017/11631-2 and 2018/21401-7, and the strategic importance of the support given by ANP (Brazil's National Oil, Natural Gas and Biofuels Agency) through the R&D levy regulation. A.F.B.B. further acknowledges financial support from FAPESP, grant numbers 2017/11937-4 and 2022/12778-5 (postdoc fellowship). The authors extend their deep appreciation for the essential contributions of both the Department of Information Technology at Campus São Carlos and the National Laboratory for Scientific Computing (LNCC/MCTI, Brazil), which were instrumental in achieving the results reported in this article.

■ REFERENCES

(1) Friend, C. M.; Xu, B. Heterogeneous Catalysis: A Central Science for a Sustainable Future. *Acc. Chem. Res.* **2017**, *50*, 517−521.
(2) Centi, G. Smart Catalytic Materials for Energy Transition. *SmartMat* **2020**, *1*, No. e1005.
(3) Bellabarba, R.; Johnston, P.; Moss, S.; Sievers, C.; Subramaniam, B.; Tway, C.; Wang, Z.; Zhu, H. Net Zero Transition: Possible Implications for Catalysis. *ACS Catal.* **2023**, *13*, 7917−7928.
(4) Harvey, B. G.; Meylemans, H. A. The Role of Butanol in the Development of Sustainable Fuel Technologies. *J. Chem. Technol. Biotechnol.* **2011**, *86*, 2−9.
(5) Pugazhendhi, A.; Mathimani, T.; Varjani, S.; Rene, E. R.; Kumar, G.; Kim, S.-H.; Ponnusamy, V. K.; Yoon, J.-J. Biobutanol as a Promising Liquid Fuel for the Future - Recent Updates and Perspectives. *Fuel* **2019**, *253*, 637−646.
(6) Jin, C.; Yao, M.; Liu, H.; Lee, C.-f. F.; Ji, J. Progress in the Production and Application of n-Butanol as a Biofuel. *Renewable Sustainable Energy Rev.* **2011**, *15*, 4080−4106.
(7) Bankar, S. B.; Survase, S. A.; Ojamo, H.; Granström, T. Biobutanol: The Outlook of an Academic and Industrialist. *RSC Adv.* **2013**, *3*, 24734−24757.
(8) Ibrahim, M. F.; Kim, S. W.; Abd-Aziz, S. Advanced Bioprocessing Strategies for Biobutanol Production from Biomass. *Renewable Sustainable Energy Rev.* **2018**, *91*, 1192−1204.
(9) Kushwaha, D.; Srivastava, N.; Mishra, I.; Upadhyay, S. N.; Mishra, P. K. Recent Trends in Biobutanol Production. *Rev. Chem. Eng.* **2019**, *35*, 475−504.
(10) Guo, Y.; Liu, Y.; Guan, M.; Tang, H.; Wang, Z.; Lin, L.; Pang, H. Production of Butanol from Lignocellulosic Biomass: Recent Advances, Challenges, and Prospects. *RSC Adv.* **2022**, *12*, 18848−18863.
(11) Kozlowski, J. T.; Davis, R. J. Heterogeneous Catalysts for the Guerbet Coupling of Alcohols. *ACS Catal.* **2013**, *3*, 1588−1600.
(12) Chieregato, A.; Velasquez Ochoa, J.; Bandinelli, C.; Fornasari, G.; Cavani, F.; Mella, M. On the Chemistry of Ethanol on Basic Oxides: Revising Mechanisms and Intermediates in the Lebedev and Guerbet reactions. *ChemSusChem* **2015**, *8*, 377−388.
(13) Tsuchida, T.; Sakuma, S.; Takeguchi, T.; Ueda, W. Direct Synthesis of n-Butanol from Ethanol over Nonstoichiometric Hydroxyapatite. *Ind. Eng. Chem. Res.* **2006**, *45*, 8634−8642.
(14) Tsuchida, T.; Yoshioka, T.; Sakuma, S.; Takeguchi, T.; Ueda, W. Synthesis of Biogasoline from Ethanol over Hydroxyapatite Catalyst. *Ind. Eng. Chem. Res.* **2008**, *47*, 1443−1452.
(15) Tsuchida, T.; Kubo, J.; Yoshioka, T.; Sakuma, S.; Takeguchi, T.; Ueda, W. Reaction of Ethanol Over Hydroxyapatite Affected by Ca/P Ratio of Catalyst. *J. Catal.* **2008**, *259*, 183−189.
(16) Ogo, S.; Onda, A.; Iwasa, Y.; Hara, K.; Fukuoka, A.; Yanagisawa, K. 1-Butanol Synthesis from Ethanol over Strontium Phosphate Hydroxyapatite Catalysts with Various Sr/P Ratios. *J. Catal.* **2012**, *296*, 24−30.
(17) Bittencourt, A. F. B.; Mendes, P. C. D.; Valença, G. P.; Da Silva, J. L. F. Acid-Base Properties of Hydroxyapatite(0001) by the Adsorption of Probe Molecules: An Ab Initio Investigation. *Phys. Rev. Mater.* **2021**, *5*, 075003.
(18) Kiani, D.; Baltrusaitis, J. Surface chemistry of hydroxyapatite for sustainable n-butanol production from bio-ethanol. *Chem Catal.* **2021**, *1*, 782−801.
(19) Veibel, S.; Nielsen, J. I. On the Mechanism of the Guerbet Reaction. *Tetrahedron* **1967**, *23*, 1723−1733.
(20) Ho, C. R.; Shylesh, S.; Bell, A. T. Mechanism and Kinetics of Ethanol Coupling to Butanol over Hydroxyapatite. *ACS Catal.* **2016**, *6*, 939−948.
(21) Diallo-Garcia, S.; Osman, M. B.; Krafft, J.-M.; Casale, S.; Thomas, C.; Kubo, J.; Costentin, G. Identification of Surface Basic Sites and Acid-Base Pairs of Hydroxyapatite. *J. Phys. Chem. C* **2014**, *118*, 12744−12757.
(22) Osman, M. B.; Krafft, J.-M.; Thomas, C.; Yoshioka, T.; Kubo, J.; Costentin, G. Importance of the Nature of the Active Acid/Base Pairs of Hydroxyapatite Involved in the Catalytic Transformation of Ethanol to n-Butanol Revealed by Operando DRIFTS. *ChemCatChem* **2019**, *11*, 1765−1778.
(23) Wang, S.-C.; Cendejas, M. C.; Hermans, I. Insights into Ethanol Coupling over Hydroxyapatite using Modulation Excitation Operando Infrared Spectroscopy. *ChemCatChem* **2020**, *12*, 4167−4175.
(24) Hohenberg, P.; Kohn, W. Inhomogeneous Electron Gas. *Phys. Rev.* **1964**, *136*, B864−B871.
(25) Kohn, W.; Sham, L. J. Self-Consistent Equations Including Exchange and Correlation Effects. *Phys. Rev.* **1965**, *140*, A1133−A1138.
(26) Perdew, J. P.; Burke, K.; Ernzerhof, M. Generalized Gradient Approximation Made Simple. *Phys. Rev. Lett.* **1996**, *77*, 3865−3868.
(27) Blöchl, P. E. Projector Augmented-Wave Method. *Phys. Rev. B: Condens. Matter Mater. Phys.* **1994**, *50*, 17953−17979.
(28) Kresse, G.; Joubert, D. From Ultrasoft Pseudopotentials to the Projector Augmented-Wave Method. *Phys. Rev. B: Condens. Matter Mater. Phys.* **1999**, *59*, 1758−1775.
(29) Kresse, G.; Hafner, J. Ab Initio Molecular Dynamics for Open-Shell Transition Metals. *Phys. Rev. B: Condens. Matter Mater. Phys.* **1993**, *48*, 13115−13118.
(30) Kresse, G.; Furthmüller, J. Efficient Iterative Schemes for Ab Initio Total-Energy Calculations Using a Plane-Wave Basis Set. *Phys. Rev. B: Condens. Matter Mater. Phys.* **1996**, *54*, 11169−11186.
(31) Grimme, S.; Antony, J.; Ehrlich, S.; Krieg, H. A Consistent and Accurate Ab Initio Parametrization of Density Functional Dispersion Correction (DFT-D) for the 94 Elements H− Pu. *J. Chem. Phys.* **2010**, *132*, 154104.
(32) Vlaisavljevich, B.; Huck, J.; Hulvey, Z.; Lee, K.; Mason, J. A.; Neaton, J. B.; Long, J. R.; Brown, C. M.; Alfè, D.; Michaelides, A.; Smit, B. Performance of van der Waals Corrected Functionals for Guest Adsorption in the M_2(dobdc) Metal−Organic Frameworks. *J. Phys. Chem. A* **2017**, *121*, 4139−4151.
(33) Freire, R. L. H.; Guedes-Sobrinho, D.; Kiejna, A.; Da Silva, J. L. F. Comparison of the Performance of van der Waals Dispersion Functionals in the Description of Water and Ethanol on Transition Metal Surfaces. *J. Phys. Chem. C* **2018**, *122*, 1577−1588.
(34) Bartaquim, E. O.; Bezerra, R. C.; Bittencourt, A. F. B.; Da Silva, J. L. F. Computational Investigation of van der Waals Corrections in the Adsorption Properties of Molecules on the Cu(111) Surface. *Phys. Chem. Chem. Phys.* **2022**, *24*, 20294−20302.

https://doi.org/10.1021/acs.jpcc.4c03937
J. Phys. Chem. C XXXX, XXX, XXX−XXX

(35) Fihri, A.; Len, C.; Varma, R. S.; Solhy, A. Hydroxyapatite: A Review of Syntheses, Structure and Applications in Heterogeneous Catalysis. *Coord. Chem. Rev.* **2017**, *347*, 48−76.
(36) Elliott, J. C. *Structure and Chemistry of the Apatites and Other Calcium Orthophosphates*; Elsevier: Amsterdam, Netherlands, 1994.
(37) Brasil, H.; Bittencourt, A. F. B.; Yokoo, K. C. E. S.; Mendes, P. C. D.; Verga, L. G.; Andriani, K. F.; Landers, R.; Da Silva, J. L. F.; Valença, G. P. Synthesis Modification of Hydroxyapatite Surface for Ethanol Conversion: The Role of the Acidic/Basic Sites Ratio. *J. Catal.* **2021**, *404*, 802−813.
(38) Hughes, J. M.; Cameron, M.; Crowley, K. D. Structural Variations in Natural F, OH, and Cl Apatites. *Am. Mineral.* **1989**, *74*, 870−876.
(39) Kim, S.; Chen, J.; Cheng, T.; Gindulyte, A.; He, J.; He, S.; Li, Q.; Shoemaker, B. A.; Thiessen, P. A.; Yu, B.; Zaslavsky, L.; Zhang, J.; Bolton, E. E. PubChem 2023 Update. *Nucleic Acids Res.* **2023**, *51*, D1373−D1380.
(40) Shustorovich, E. M. Dissociation activation barrier and heat of chemisorption: A Morse-type analytical approach. *Surf. Sci. Lett.* **1985**, *150*, L115−L121.
(41) Shustorovich, E. Chemisorption Phenomena: Analytic Modeling Based on Perturbation Theory and Bond-Order Conservation. *Surf. Sci. Rep.* **1986**, *6*, 1−63.
(42) Shustorovich, E.; Sellers, H. The UBI-QEP Method: A Practical Theoretical Approach to Understanding Chemistry on Transition Metal Surfaces. *Surf. Sci. Rep.* **1998**, *31*, 1−119.
(43) Van Belleghem, J.; Yang, J.; Janssens, P.; Poissonnier, J.; Chen, D.; Marin, G. B.; Thybaut, J. W. Microkinetic Model Validation for Fischer−Tropsch Synthesis at Methanation Conditions Based on Steady State Isotopic Transient Kinetic Analysis. *J. Ind. Eng. Chem.* **2022**, *105*, 191−209.
(44) Ahmad, K.; Abi Jaoude, M.; Upadhyayula, S.; Polychronopoulou, K.; Ravaux, F. Kinetics of Greenhouse Gas CO_2 Hydrogenation Over K-promoted Cu/ZnO/Cr_2O_3 Catalyst Towards Sustainable Aviation Fuel Production. *Fuel* **2023**, *337*, 127250.
(45) Durán-Pérez, J.; Rivera de la Cruz, J. G.; Castillo-Araiza, C. O. Elucidating Selective and Total Oxidation Elementary Reactions over a Ni-Based Catalyst for Sustainable Ethylene Production via Oxidative Dehydrogenation of Ethane: Microkinetic Analysis. *Chem. Eng. J.* **2023**, *470*, 143939.
(46) Moraes, P. I. R.; Bittencourt, A. F. B.; Andriani, K. F.; Da Silva, J. L. F. Theoretical Insights into Methane Activation on Transition-Metal Single-Atom Catalysts Supported on the CeO_2(111) Surface. *J. Phys. Chem. C* **2023**, *127*, 16357−16366.
(47) Al-Mahayni, H.; Wang, X.; Harvey, J.-P.; Patience, G. S.; Seifitokaldani, A. Experimental Methods in Chemical Engineering: Density Functional Theory. *Can. J. Chem. Eng.* **2021**, *99*, 1885−1911.
(48) Jensen, J. H. Predicting Accurate Absolute Binding Energies in Aqueous Solution: Thermodynamic Considerations for Electronic Structure Methods. *Phys. Chem. Chem. Phys.* **2015**, *17*, 12441−12451.
(49) Wang, V.; Xu, N.; Liu, J.-C.; Tang, G.; Geng, W.-T. VASPKIT: A User-Friendly Interface Facilitating High-Throughput Computing and Analysis Using VASP Code. *Comput. Phys. Commun.* **2021**, *267*, 108033.
(50) Larsen, A. H.; Mortensen, J. J.; Blomqvist, J.; Castelli, I. E.; Christensen, R.; Dułak, M.; Friis, J.; Groves, M. N.; Hammer, B.; Hargus, C.; Hermes, E. D.; Jennings, P. C.; Jensen, P. B.; Kermode, J.; Kitchin, J. R.; Kolsbjerg, E. L.; Kubal, J.; Kaasbjerg, K.; Lysgaard, S.; Maronsson, J. B.; Maxson, T.; Olsen, T.; Pastewka, L.; Peterson, A.; Rostgaard, C.; Schiøtz, J.; Schütt, O.; Strange, M.; Thygesen, K. S.; Vegge, T.; Vilhelmsen, L.; Walter, M.; Zeng, Z.; Jacobsen, K. W. The Atomic Simulation Environment—A Python Library for Working with Atoms. *J. Phys.: Condens. Matter* **2017**, *29*, 273002.
(51) Moteki, T.; Flaherty, D. W. Mechanistic Insight to C− C Bond Formation and Predictive Models for Cascade Reactions among Alcohols on Ca- and Sr-Hydroxyapatites. *ACS Catal.* **2016**, *6*, 4170−4183.
(52) Zhou, B.-C.; Li, W.-C.; Lv, W.-L.; Xiang, S.-Y.; Gao, X.-Q.; Lu, A.-H. Enhancing Ethanol Coupling to Produce Higher Alcohols by Tuning H_2 Partial Pressure over a Copper-Hydroxyapatite Catalyst. *ACS Catal.* **2022**, *12*, 12045−12054.
(53) Xue, M.; Yang, B.; Xia, C.; Zhu, G. Upgrading Ethanol to Higher Alcohols via Biomass-Derived Ni/Bio-Apatite. *ACS Sustainable Chem. Eng.* **2022**, *10*, 3466−3476.
(54) Motagamwala, A. H.; Dumesic, J. A. Microkinetic Modeling: A Tool for Rational Catalyst Design. *Chem. Rev.* **2021**, *121*, 1049−1076.
(55) Wang, W.-Y.; Wang, G.-C. Nickel/Molybdenum Bimetallic Alloy for Dry Reforming of Methane: A Coverage-Dependence Microkinetic Model Simulation Based on the First-Principles Calculation. *J. Phys. Chem. C* **2021**, *125*, 18653−18664.
(56) Houston, P. L. *Chemical Kinetics and Reaction Dynamics*; Dover Publications: Mineola, NY, 2006.
(57) Virtanen, P.; Gommers, R.; Oliphant, T. E.; Haberland, M.; Reddy, T.; Cournapeau, D.; Burovski, E.; Peterson, P.; Weckesser, W.; Bright, J.; van der Walt, S. J.; Brett, M.; Wilson, J.; Millman, K. J.; Mayorov, N.; Nelson, A. R. J.; Jones, E.; Kern, R.; Larson, E.; Carey, C. J.; Polat, I.·.; Feng, Y.; Moore, E. W.; VanderPlas, J.; Laxalde, D.; Perktold, J.; Cimrman, R.; Henriksen, I.; Quintero, E. A.; Harris, C. R.; Archibald, A. M.; Ribeiro, A. H.; Pedregosa, F.; van Mulbregt, P.; et al. SciPy 1.0: Fundamental Algorithms for Scientific Computing in Python. *Nat. Methods* **2020**, *17*, 261−272.
(58) Hanspal, S.; Young, Z. D.; Shou, H.; Davis, R. J. Multiproduct Steady-State Isotopic Transient Kinetic Analysis of the Ethanol Coupling Reaction over Hydroxyapatite and Magnesia. *ACS Catal.* **2015**, *5*, 1737−1746.

https://doi.org/10.1021/acs.jpcc.4c03937
J. Phys. Chem. C XXXX, XXX, XXX−XXX